Towards three-body unitarity in $D^+ \rightarrow K^- \pi^+ \pi^+$

P. C. Magalhães,[1,*] M. R. Robilotta,[1] K. S. F. F. Guimarães,[2] T. Frederico,[2,†] W. de Paula,[2] I. Bediaga,[3] A. C. dos Reis,[3,‡]
C. M. Maekawa,[4] and G. R. S. Zarnauskas[§]

[1]*Instituto de Física, Universidade de São Paulo, São Paulo, SP, Brazil, 05315-970*
[2]*Instituto Tecnológico de Aeronáutica, São José dos Campos, SP, Brazil, 12.228-900*
[3]*Centro Brasileiro de Pesquisas Físicas, Rio de Janeiro, RJ, Brazil, 22290-180*
[4]*Instituto de Matemática, Estatística e Física, Universidade Federal do Rio Grande,*
Rio Grande, RS, Brazil; Campus Carreiros, PO Box 474, 96201-900

We assess the importance of final state interactions in $D^+ \rightarrow K^- \pi^+ \pi^+$, stressing the consistency between two- and three-body interactions. The basic building block in the calculation is a $K\pi$ amplitude based on unitarized chiral perturbation theory and with parameters determined by a fit to elastic LASS data. Its analytic extension to the second sheet allows the determination of two poles, associated with the κ and the $K^*(1430)$, and a representation of the amplitude based on them is constructed. The problem of unitarity in the three-body system is formulated in terms of an integral equation, inspired in the Faddeev formalism, which implements a convolution between the weak vertex and the final state hadronic interaction. Three different topologies are considered for the former and, subsequently, the decay amplitude is expressed as a perturbation series. Each term in this series is systematically related to the previous one and a resummation was performed. Remaining effects owing to single and double rescattering processes were then added and results compared to FOCUS data. We found that proper three-body effects are important at threshold and fade away rapidly at higher energies. Our model, based on a vector-weak vertex, can describe qualitative features of the modulus of the decay amplitude and agrees well with its phase in the elastic region.

I. MOTIVATION

About 40 years ago, reactions of the type $KN \rightarrow \pi KN$ were used to determine the $K\pi$ amplitude [1]. Such reactions involve the scattering of an incoming kaon and a pion from the nucleon cloud. The dominant one-pion exchange amplitude is isolated by selecting events with low momentum transfer. This is the only $K\pi \rightarrow K\pi$ scattering data, collected in the range $0.825 < m_{K\pi} < 1.96$ GeV/c^2.

In the past decade, heavy flavor decays, in particular, decays of D mesons, became a key to the physics of the light scalars. Currently, these are the only process in which S-wave amplitudes can be continuously studied, starting from threshold, filling the existing gaps on the scattering data. In addition, very large, high-purity samples, in which the initial state has always well defined quantum numbers, became available in the past few years. Multibody decays of heavy flavor particles proceed almost entirely via intermediate states involving resonances that couple to $\pi\pi$ and $K\pi$. The universal $K\pi$ and $\pi\pi$ amplitudes are, therefore, present in these decays as well. These amplitudes could, in principle, be extracted with great precision.

Most of the existing results come from hadronic decays of D mesons. The golden modes are the D^+, $D_s^+ \rightarrow \pi^- \pi^+ \pi^+$ [2] and, in the case of the $K\pi$ system, the $D^+ \rightarrow K^- \pi^+ \pi^+$ [3] decay. These decay modes share some common features: the presence of two identical particles in the final state and a largely dominant S-wave component. The standard procedure is the analysis of the Dalitz plot, in which the decay amplitude is modeled by a coherent sum of resonant amplitudes, accounting for the possible intermediate states—the so-called isobar model. The extraction of the resonance parameters and decay fractions, however, depends strongly on the particular model used for the S wave.

The situation concerning the experimental results on the $K\pi$ amplitude is intriguing. The S-wave amplitude can be also studied with semileptonic decays. In principle, in decays such as $D \rightarrow K\pi l\nu_l$ or $\tau \rightarrow K\pi\nu_\tau$, the extraction of the S wave would be simpler than in the case of hadronic decays, for the $K\pi$ system is free from final state interactions (FSIs) with the lepton pair. The $K\pi$ S wave, in this case, should match that of LASS [1], provided no energy-dependent phase is inherited from the weak decay vertex. The results are conflicting, though. While the *BABAR* analysis of the decay $D^+ \rightarrow K^- \pi^+ e^+ \nu_e$ [4] and the FOCUS analysis of the decay $D^+ \rightarrow K^- \pi^+ \mu^+ \nu_\mu$ [5] conclude that the $K\pi$ amplitude is consistent with the LASS results, the analysis of the decay $\tau^- \rightarrow \overline{K}^0 \pi^- \nu_\tau$, carried out by the

*patricia@if.usp.br
†tobias@ita.br
‡alberto@cbpf.br
§Present address: Wibichstrasse 20, 3087 Zurich, Switzerland

BABAR and Belle Collaborations [6,7] showed that these data cannot be described by the LASS amplitude.

In 2006, the E791 Collaboration published a model independent analysis of the $K^-\pi^+$ S-wave amplitude using the $D^+ \to K^-\pi^+\pi^+$ decay [8]. A very similar analysis was performed by the FOCUS Collaboration [9]. The CLEO-c Collaboration also studied this decay, but with a somewhat different method [10]. In the E791 approach, the S-wave $K^-\pi^+$ amplitude is represented by an unknown complex function of the $K^-\pi^+$ mass, to be determined directly from the data. The P and D wave were parameterized by the usual sum of Breit-Wigner amplitudes. The $K^-\pi^+$ mass spectrum was uniformly divided into 40 bins. In each bin the S-wave amplitude was defined by two real numbers, $\mathcal{A}_0(m^j_{K\pi}) = a^j_0 e^{i\delta^j}$. The set of 40 pairs (a^j_0, δ^j) (80 free parameters) define the S wave through the entire $K\pi$ spectrum. The phase and magnitude of the S wave at an arbitrary position were obtained by a cubic spline interpolation.

The $K^-\pi^+$ S-wave amplitude obtained by E791 and FOCUS is significantly different from that from LASS. Possible explanations for this discrepancy fall into two broad categories, and the first one concerns the weak vertex. In the hadronic scale, the mass of the D is far from both chiral and heavy quark limits, and the treatment of its decays cannot be simplified by the techniques developed in these realms [11]. The second class of effects concerns strong interactions, which do take place after the weak decay. The treatment of this part of the problem is necessarily involved since, even in its simplest version, these FSIs already involve three bodies (see, e.g. [12]). Other examples of the importance of final state interactions in three-body decays of heavy mesons can be found in [13–15]. As the final mesons are light and have high energies, kinematics is fully relativistic, and techniques developed in low-energy Nuclear Physics, for the treatment of three-body systems, do not apply. In the case of relativistic Particle Physics, in spite of a growing literature [16,17], the corresponding techniques are still in the want of being developed for the application to the decay problem. Approaches to the relativistic few-body systems (two- and three-body) have been collected in a series of works that presents the main developments done so far (see Refs. [18–24]). The weak vertex of $D^+ \to K^-\pi^+\pi^+$ was treated by means of factorization and form factors, supplemented by two-body final state interactions [25,26].

In this work, we concentrate on the three-body structure of strong dynamics of FSIs and postpone a detailed discussion of the weak vertex. As one knows little about this problem, our aim is to identify leading effects, and a number of simplifications are made. Hopefully, once these leading effects are understood, corrections can be included in a systematic way.

Our discussion of three-body FSIs is based on the theoretical framework provided by chiral symmetry in the $SU(3)$ sector to describe the two-meson scattering

amplitude. At low energies, chiral perturbation theory (ChPT) yields the most reliable representation of QCD [27,28]. In the present problem, Dalitz plots for $D^+ \to K^-\pi^+\pi^+$ involve energies in the range $0.4 \le M^2_{i2} \le 3$ GeV, where the K is taken as particle 2, adopting Particle Data Group [29] convention. The low-energy end of this range is directly within the scope of ChPT, and it is in this region where discrepancies between LASS [1] and FOCUS [9] data are more pronounced. Even outside this range, the chiral framework still proves to be very useful and provides rigorous guidance for possible extensions.

The case of the κ is paradigmatic. This state was found in a number of experiments [3,8–10,30] and theoretical models [31–34], with a complex mass $m_\kappa = [(0.672 \mp 0.040) - i(0.550 - 0.034)]$ GeV [29], which can be considered as low in the hadronic scale. For this very reason, it definitely cannot be accommodated as a fundamental resonance in a chiral Lagrangian [28]. In ChPT, resonances can only be introduced as next-to-leading order, which decay by means of explicit couplings to pseudoscalar mesons. In this framework, a resonance should become a stable particle when its coupling to the $K\pi$ system is turned off.

The κ does not fall in this category. Its relationship with ChPT is a more subtle one and has been clarified about a decade ago [32], with the realization that unitarization of low-energy chiral results gives rise to amplitudes which have poles in the complex s plane. The κ corresponds to the state with the lowest energy, and it is present even if one considers only leading-order contact interactions (see, for instance, our Fig. 1). This idea proved to be very fruitful and motivated both reanalysis of low-energy experimental $K\pi$ data [33,34] and the interpretation of the κ as a tetraquark or two-meson state [35]. The case of the σ meson, which occurs in $SU(2)$, is totally similar (see, e.g. [36–38]). There, however, the availability of precision data allows the pole to be extracted directly from the $\pi\pi$ amplitude, in a model-independent way [39].

Our presentation is divided as follows. In Sec. II, we review, for the sake of completeness, chiral results for the $K\pi$ amplitude and its unitarization. The conceptual
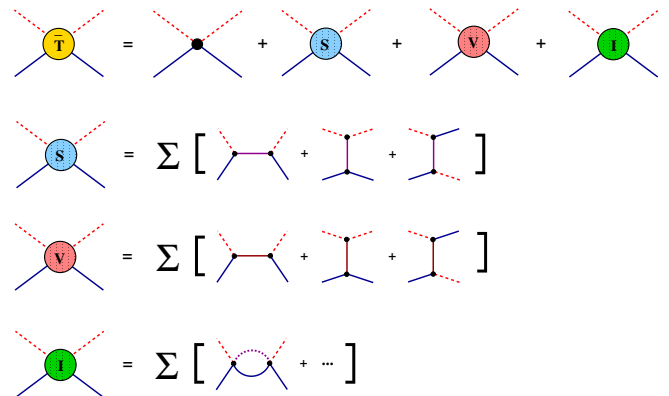

FIG. 1 (color online).   A single pole in $|D(s)|$ in the complex s plane.

framework for the three-body unitarization is introduced in Sec. III, and, in Sec. IV, its perturbative expansion is used to derive predictions for the $D^+ \rightarrow K^- \pi^+ \pi^+$ amplitude. Results and conclusions are given in Sec. V. The manuscript also includes several appendices dealing with technical matters.

II. $\bar{K}\pi$ AMPLITUDE

A. Interaction kernel

The reaction $\pi_a(p_a)\bar{K}_b(p_b) \rightarrow \pi_c(p_c)\bar{K}_d(p_d)$ is described in terms of the usual Mandelstam variables s, t, u, constrained by the condition $s + t + u = p_a^2 + p_b^2 + p_c^2 + p_d^2$. In the center of mass, results can be expressed in terms of the momentum $\boldsymbol{q}$, with $\boldsymbol{q}^2 = s\rho^2/4$, $\rho = \sqrt{1 - 2(M_\pi^2 + M_K^2)/s + (M_\pi^2 - M_K^2)^2/s^2}$.

Chiral perturbation theory determines the tree amplitudes $\bar{T}_I$, with isospin I, as the sum of a $\mathcal{O}(q^2)$ contact term [27], supplemented by $\mathcal{O}(q^4)$ scalar and vector resonances [28], together with inelastic contributions [33]. The amplitude for each channel, indicated in Fig. 2, is then written as

$$\bar{T}_I = \bar{T}^c + \bar{T}^S + \bar{T}^V + \bar{T}^I. \tag{1}$$

In this exploratory work, we are interested in determining dominant structures in the scalar sector and, in the sequence, we neglect vector resonances and inelasticities. As shown in Fig. 2, scalar resonances contribute to s, t, and u channels. Each of the corresponding amplitudes has the form $\bar{T}^S(x) = \alpha_x(x)/(x - m_x^2)$, where $x = s, t, u$, α_x is a $\mathcal{O}(q^4)$ polynomial, and m_x, a large resonance mass. In the physical region, the variables t and u are negative, whereas s is positive. This means that $\bar{T}^S(s)$ can become arbitrarily large, whereas $\bar{T}^S(t)$ and $\bar{T}^S(u)$ remain always finite. Close
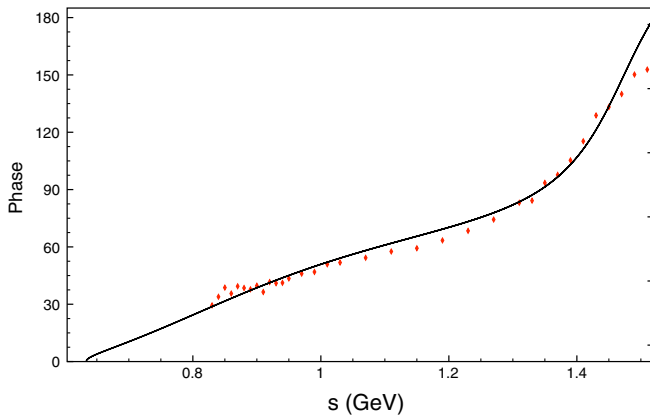

FIG. 2 (color online). $K\pi$ amplitude: the contact diagram is the leading one at low energies, whereas blobs are corrections due to other intermediate states; S and V correspond to scalar and vector resonances and I to inelastic channels; the summation signs indicate the possibility of more than one intermediate state of each kind.

to threshold, on the other hand, all the $\bar{T}^S(x)$ are smaller, by construction, than the contact term $\bar{T}^c$. Therefore, in the entire physical region, the combination $\bar{T}^S(t) + \bar{T}^S(u)$ can be neglected in comparison with $\bar{T}^c + \bar{T}^S(s)$. We thus identify the leading tree $K\pi$ amplitudes with the functions

$$\bar{T}_{1/2} = \frac{1}{F^2}[s + 3t/4 - (M_\pi^2 + M_K^2)] - \sum_i^N \frac{\alpha_i(s)}{s - m_i^2}, \tag{2}$$

$$\alpha_i = \frac{3}{2F^4}[c_d^i s - (c_d^i - c_m^i)(M_\pi^2 + M_K^2)]^2, \tag{3}$$

$$\bar{T}_{3/2}^c = -\frac{1}{2F^2}[s - (M_\pi^2 + M_K^2)], \tag{4}$$

where F is the meson decay constant and N is the number of scalar resonances of the $J^P = 0^+$ considered, with masses m_i and coupled to two mesons by the constants c_d^i and c_m^i, estimated in Ref. [28]. Their values are such that $c_d \sim c_m$ and $(c_d c_m/m_i^2) \sim 10^{-3}$, explaining why $\bar{T}^S(t)$ and $\bar{T}^S(u)$ are much smaller than the terms kept in Eq. (2). The neglect of these terms allows the $K\pi$ amplitude to be unitarized in a very compact form, as discussed in the sequence. The $I = 3/2$ amplitude is repulsive, contributes little to FSIs, and is also neglected in the sequence. Projecting out the S wave, one finds the leading kernel of the dynamical equation, given by

$$\mathcal{K}_{S_{1/2}} \equiv \mathcal{K} = \mathcal{K}_c - \sum_i^N \frac{\alpha_i(s)}{s - m_i^2}, \tag{5}$$

$$\mathcal{K}_c = [5s/8 - (M_\pi^2 + M_K^2)/4 - 3(M_\pi^2 - M_K^2)^2/8s]/F^2. \tag{6}$$

This kernel is real and hence suited for describing elastic processes only. The inclusion of inelasticities, due mostly to intermediate states containing η_1 and η_8, can be performed by means of well known coupled-channels techniques [33]. We remain within the elastic approximation and derive T, the elastic $I = 1/2$, S-wave πK scattering amplitude, by means of the Bethe-Salpeter equation, written schematically as

$$T(s) = \mathcal{K}(s) - i \int \frac{d^4\ell}{(2\pi)^4} \mathcal{K}(p,\ell) \frac{1}{[(\ell + p/2)^2 - M_\pi^2 + i\epsilon]}$$
$$\times \frac{T(p,\ell)}{[(\ell - p/2)^2 - M_K^2 + i\epsilon]}, \tag{7}$$

with $p^2 = s$. Our approximations ensure that both $\mathcal{K}$ and T do not depend on ℓ, and the Bethe-Salpeter equation acquires the very simple form

$$T = [1 - T\Omega]\mathcal{K}, \tag{8}$$

where the two-meson propagator is

$$\Omega(s) = i \int \frac{d^4\ell}{(2\pi)^4} \frac{1}{[(\ell + p/2)^2 - M_\pi^2 + i\epsilon]}$$
$$\times \frac{1}{[(\ell - p/2)^2 - M_K^2 + i\epsilon]}. \tag{9}$$

This integral is ultraviolet divergent, but this unwanted behavior can be cured by means of a subtraction. Following Ref. [27], we write the regular part of Ω as

$$\bar{\Omega}(s) = \Omega(s) - \Omega(0), \tag{10}$$

where the divergent part of $\Omega(s)$ is contained in $\Omega(0)$. Regularization amounts to the replacement $\Omega(0) \rightarrow C$, where C is an unknown finite constant which has to be fixed by experimental input. The function $\bar{\Omega}$ can be evaluated analytically, and explicit results are given in Appendix A. After regularization, Eq. (8) becomes

$$T = [1 - T(C + \bar{\Omega})]\mathcal{K}, \tag{11}$$

and its solution reads

$$T = \mathcal{K}/D, \tag{12}$$

$$D = 1 + (C + \bar{\Omega})\mathcal{K}. \tag{13}$$

The $K\pi$ amplitude is thus determined by a rather simple algebraic equation, involving just the two-meson propagator and the kernel. The latter, in turn, includes only contact interactions and s-channel resonances. In the sequence, we will use the result

$$T(C + \bar{\Omega}) = 1 - 1/D, \tag{14}$$

derived from Eq. (12). The function $\bar{\Omega}$ is real below the threshold at $s = (M_\pi + M_K)^2$ and acquires an imaginary component above it. In the physical region, below the first inelastic threshold, the kernel is real, whereas $\bar{\Omega} = \bar{\Omega}_R + i\bar{\Omega}_I$, $\bar{\Omega}_I = -\rho/16\pi$, and the unitary amplitude can be represented by means of a real phase shift δ [40] as

$$T = \frac{16\pi}{\rho} \sin\delta e^{i\delta} \leftrightarrow \tan\delta = -\frac{\bar{\Omega}_I\mathcal{K}}{1 + (C + \bar{\Omega}_R)\mathcal{K}}. \tag{15}$$

For energies above inelastic thresholds, the kernel $\mathcal{K}$ acquires imaginary components owing to processes included in the blob I of Fig. 2, and the amplitude is damped.

B. Alternative representations

As a side comment, we note that the representation of T, in terms of Breit-Wigner structures, is not suited to this problem. They apply just to a single isolated resonance, since Eq. (5) would read $\mathcal{K} = -\alpha_1/(s - m_1^2)$, and Eq. (12) could be written as

$$T = \frac{-\alpha_1}{s - [m_1^2 + (C + \bar{\Omega}_R)\alpha_1] + i[\rho\alpha_1/16\pi]}. \tag{16}$$

In this case, the terms $m_1^2 + (C + \bar{\Omega}_R)\alpha_1$ and $\rho\alpha_1/16\pi$ could be identified as a running mass and a width, respectively. On the other hand, in the more realistic situation where both the contact interaction and other resonances are present, the coupled structure of the problem shows up. For instance, in the case of a contact term supplemented by two resonances, the amplitude (12) would read

$$T = \frac{(s - m_1^2)(s - m_2^2)\mathcal{K}_c - (s - m_2^2)\alpha_1 - (s - m_1^2)\alpha_2}{1 + (C + \bar{\Omega}_R + i\bar{\Omega}_I)[\mathcal{K}_c - \alpha_1/(s - m_1^2) - \alpha_2/(s - m_1^2)]}$$
$$\times \frac{1}{(s - m_1^2)(s - m_2^2)}. \tag{17}$$

The coupling of various types of interaction gives rise to a complicated structure which cannot be written naturally as either products or sums of individual Breit-Wigner expressions for each resonance.

C. Data and poles-schematic features

The main qualitative features of the FSIs can be understood by means of a $K\pi$ amplitude as given just by a chiral contact term, supplemented by a single resonance. When more resonances are included, these features are preserved, but the amount of algebraic work increases considerably. We work with the simplest version, which corresponds to

$$T = \frac{\mathcal{K}}{1 + (C + \bar{\Omega})\mathcal{K}}, \qquad \mathcal{K} = \mathcal{K}_c - \alpha_1/(s - m_1^2). \tag{18}$$

This amplitude depends on two sets of 3 parameters, namely F, M_π, M_K and m_1, c_d^1, c_m^1, besides the subtraction constant C. The first set is determined by chiral perturbation theory, and we adopt $F = \sqrt{F_\pi F_K} = 0.102722$ GeV [33], $M_\pi^+ = 0.1396$ GeV, and $M_K^+ = 0.4937$ GeV. The other one is obtained by fitting LASS data [1] in the elastic region, and we find $C = -1 \times 10^{-3}$, $m_1 = 1.33$ GeV, $c_d^1 = 0.0352$ GeV, and $c_m^1 = 0.001027$ GeV, which yield the curve shown in Fig. 3. Results for the coupling constants are close to 1 of the sets given in Ref. [33] $[c_d, c_m = 0.030, 0.043]$ GeV and roughly consistent with those derived from the decay $a_0 \rightarrow \eta\pi$ in Ref. [28], namely $c_d = 0.032$ GeV and $c_m = 0.042$ GeV.

Feeding the parameters from the fit into Eq. (18) and extending it to the second Riemann sheet, one finds two coupled poles in the complex s plane, given by the condition $D(s) = 0$. They are located at $s = \theta_i$, with $\theta_\kappa = 0.51426725 - i0.51423116$ GeV^2 and $\theta_1 = 2.16256534 - i0.24130498$ GeV^2, and identified, respectively, with the κ and the $K_0^*(1430)$. The latter is compatible with the Particle Data Group [29] value, $s_{(1430)} = [(2.01 \pm 0.15) - i(0.38 \pm 0.13)]$ GeV^2. In order to produce a feeling for
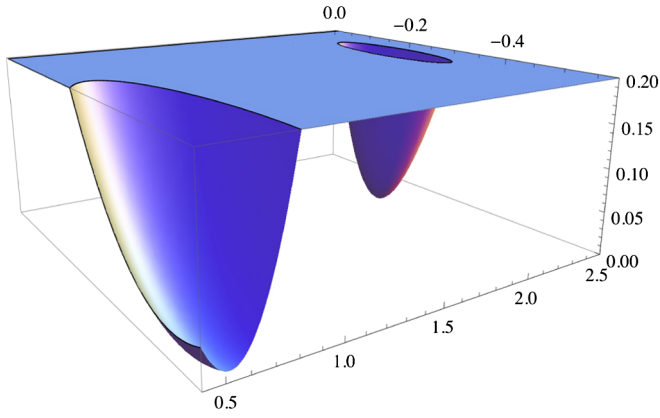
FIG. 3 (color online). S-wave isospin 1/2 phase shift: LASS data [1] and our fit.

FIG. 5 (color online). (color online) Real (full lines) and imaginary (dashed lines) components of the $K\pi$ amplitude from Eq. (18) (blue) and the pole representation, labeled PR, Eq. (19) (red).

the strength of the coupling between these resonances, we keep just the contact term in Eq. (18), by setting $\alpha_1 = 0$, finding $\theta_\kappa = 0.45505779 - i0.51167711 \text{ GeV}^2$, and $\theta_1 = m_1^2$. The κ pole is thus rather stable. The behavior of the function $D(s)$ along the complex s plane is shown in Fig. 4, and it is possible to see two wells around the κ and $K_0^*(1430)$ poles. The plot in Fig. 1 corresponds to the case $\alpha_1 = 0$, in which just the κ exists, dynamically generated.

The fact that the function $D(s)$ has two poles in the second Riemann sheet allows the elastic amplitude, Eq. (12), to be represented as

$$T = \frac{\mathcal{K}}{D} = \mathcal{K}\left[\beta + \frac{\gamma_\kappa}{s - \theta_\kappa} + \frac{\gamma_1}{s - \theta_1}\right], \quad (19)$$

with $\beta = 0.22$, $\gamma_\kappa = -0.1849 + i0.6378 \text{ GeV}^2$, $\gamma_1 = 0.2247 + i0.1260 \text{ GeV}^2$. In Fig. 5, we compare it with the exact amplitude and learn that this simple representation is reasonable in the range covered by the Dalitz plot. We adopt it in the present exploratory work and leave a more complete treatment for a future investigation.
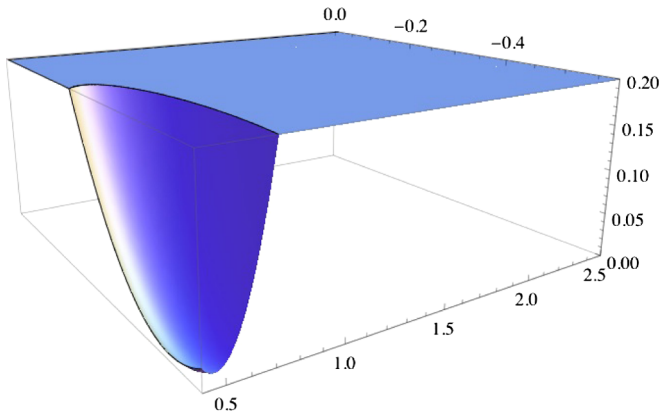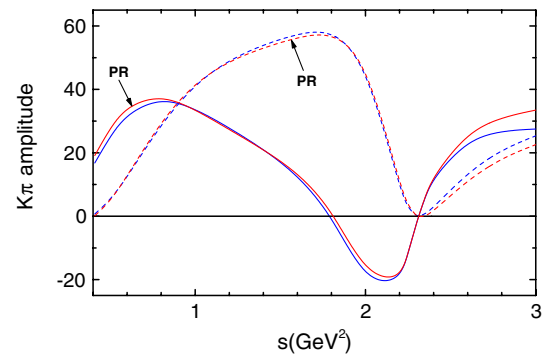

FIG. 4 (color online). Two poles in $|D(s)|$ in the complex s plane.

III. THREE-BODY UNITARITY

The amplitude $D^+ \to K^-\pi^+\pi^+$, denoted by $A(m_{12}^2, m_{23}^2)$, is symmetric under the exchange of the final pions and written as

$$A(m_{12}^2, m_{23}^2) = W(m_{12}^2, m_{23}^2) + a(m_{12}^2) + a(m_{23}^2), \quad (20)$$

where W is the weak vertex, and the functions a incorporate hadronic FSIs.

In Figs. 6 and 7, we show the structure of A in terms of the rescattering series, which depends on T, the $K\pi$ amplitude obtained in the preceding section. The diagram involving just W in Fig. 6 describes the possibility that the mesons produced in the decay reach the detector without interacting. As the Fermi coupling constant G_F entering W is very small, the amplitude $A(m_{12}^2, m_{23}^2)$ is linear in this parameter, indicating that each dynamical component of the weak vertex in Fig. 6 evolves independently by means of FSIs. In other words, if the primary vertex can be written as a sum $W = \sum_i W_{(i)}$ of dynamical contributions, one automatically has $A = \sum_i A_{(i)}$.

In principle, $\pi^+\pi^+$ interactions could contribute to FSIs, but this subsystem has isospin 2, and this channel can be safely neglected because phase shifts are small. Three-body unitarity is then dominated by the series represented in Fig. 7, where the first diagram corresponds to
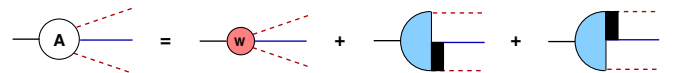

FIG. 6 (color online). Diagrammatic representation of the heavy meson decay process into $K\pi\pi$, starting from the partonic amplitude (red) and adding hadronic multiple scattering in the ladder approximation.
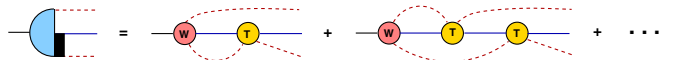

FIG. 7 (color online). Rescattering series implementing three-body unitary.

the spectator-pion approximation, often found in the literature. Contributions from the three-body irreducible rescattering process are terms of the series which contain successive interactions among different pairs. The second diagram is thus the lowest order contribution of this kind.

In this work, we concentrate on the perturbative structure of the series describing strong final state interactions. In order to perform such a study, one needs information concerning the production of the $K\pi\pi$ system in the primary weak decay. A suitable conceptual point of departure is the quark diagram approach described by Chau [41], based on 6 independent topologies. In spite of their symbolic character and the absence of interactions mediated by gluons, they implement properly the Cabibbo-Kobayashi-Maskawa quark mixing. In the specific case of nonleptonic D decays, leading contributions are incorporated into the hadronic effective Lagrangian given by Bauer, Stech, and Wirbel [42] as

$$L_{\text{eff}} = \frac{G_F}{\sqrt{2}}\{a_1(\bar{u}d')_H(\bar{s}'c)_H + a_2(\bar{s}'d')_H(\bar{u}c)_H\}, \quad (21)$$

where $(\bar{q}q)_H$ represents hadronic expectation values of $V - A$ charged weak currents and, the QCD factors $a1$ and $a2$ are related to the Wilson coefficients with ratio roughly given by $a_2/a_1 \sim -0.4$. A detailed study of the process $D^+ \to K^-\pi^+\pi^+$ based on this Lagrangian has been performed by Boito and Escribano [25], considering two-body FSIs only. These authors assessed the relative importance of contributions proportional to either a_1 or a_2 to observables, and the latter was found to be rather visible, although systematically smaller than the former. In this work, we focus on the strong evolution of leading contributions and neglect, for the moment, the color-suppressed term proportional to a_2. The light quark sector in the term proportional to a_1 involves just $(\bar{u}d)_H$, which is minimally realized by the matrix elements $\langle\pi^+|A^+|0\rangle$ and $\langle\pi^0\pi^+|V^+|0\rangle$. Concerning the factor $(\bar{s}c)_H$, we allow the final strange quark to be carried by either a kaon or a strange scalar resonance and arrive at the set of topologies indicated schematically in Fig. 8. The strengths of these vertices are respectively W_a, W_b, and W_c, assumed provisionally as constants. In the case of W_a, one has the isospin substructure: $K^-(k)\pi^+(q)\pi^+(q') \to \sqrt{2/3}W_a$ and $\bar{K}^0(k)\pi^0(q)\pi^+(q') \to -\sqrt{1/3}W_a$.

The construction of the amplitudes $a(m_{i2}^2)$ is discussed in the sequence and formulated in terms of the rather general
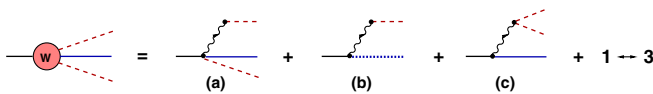

FIG. 8 (color online). Topologies for the weak vertex: the dotted line is a scalar resonance and the wavy line is a W^+, which is contracted to a point in calculation; in diagram c, one of the pions is neutral.

$K\pi$ amplitude given by Eq. (12). Hence, it does not depend on values adopted for parameters, on the number of explicit resonances considered, or on possible couplings to inelastic channels. The function $a(m_{12}^2)$ is written as

$$a(m_{12}^2) = \sum_{N=1}^{\infty} a_N(m_{12}^2), \quad (22)$$

where N is the number of $K\pi$ amplitudes intervening in a particular diagram of Fig. 7. The sum in Eq. (22) can be performed by means of a Faddeev-like decomposition of the amplitude $A(m_{12}^2, m_{23}^2)$. The Faddeev components are identified with $a(m_{12}^2)$ and $a(m_{23}^2)$, which are the nonperturbative solution of a scattering equation.

Following the model proposed in Ref. [16], we write the full decay amplitude of Fig. 7 as

$$A(m_{12}^2, m_{23}^2) = W\left[1 - \int\frac{d^4q\,d^4q'}{(2\pi)^8}\frac{T_{3\to 3}(k, k'; q, q')}{(q^2 - M_\pi^2 + i\epsilon)}\right.$$
$$\left.\times\frac{1}{(q'^2 - M_\pi^2 + i\epsilon)[(P - q' - q)^2 - M_K^2 + i\epsilon]}\right],$$
$$(23)$$

where P, k, and k' are, respectively, the momenta of the D and of the pions produced in its decay. The matrix element of the $3 \to 3$ transition matrix is $T_{3\to 3}(k, k'; q, q')$. In order to simplify the description, we use the pointlike weak vertex.

The weak vertex for the decay of the D meson into the $K\pi\pi$ channel is convoluted with the $3 \to 3$ off-shell transition matrix, which takes into account the three-meson interacting final state, as shown in Fig. 7, including the three-body connected ladder series, where the $2 \to 2$ scattering process is summed up in the $K\pi$ transition matrix.

The $3 \to 3$ transition matrix is obtained from the following assumptions: i) the $K\pi\pi$ Bethe-Salpeter equation is solved in the ladder approximation, and ii) the $K\pi$ transition matrix is effective in the S-wave states. The full $3 \to 3$ ladder scattering series is summed up when the integral equations for the Faddeev decomposition of the scattering matrix are solved.

The matrix elements of our $K\pi$ amplitude depend just on the Mandelstam variable s of the two-body subsystem, as given by Eq. (8), allowing the Faddeev components of the decay amplitude to be written in a factorized form:

$$a(m_{12}^2) = T(m_{12}^2)\xi(p_3). \quad (24)$$

The function $a(m_{12}^2)$ thus carries the full effect of the final state interaction through the two-meson amplitude T multiplied by a spectator amplitude ξ, which contains the full three-body rescattering contributions, given by the sum of all processes in the ladder approximation for the multiple scattering series.

The resummation of the scattering series in the reduced amplitude $\xi(k)$ can be done by an integral equation corresponding to Fig. 9, given by
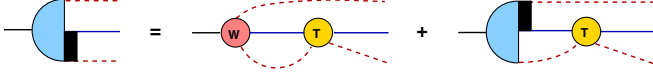
FIG. 9 (color online). Diagrammatic representation of the integral equation for the three-body function $T(m_{12}^2)\xi(k_3)$ (left). The driving term contains the partonic amplitude from the weak vertex convoluted with the two-body scattering amplitude (right, first graph).

$$\xi(k) = \xi_1(k) - i \int \frac{d^4q}{(2\pi)^4} \frac{T[(P-q)^2]}{(q^2 - M_\pi^2 + i\epsilon)}$$
$$\times \frac{\xi(q)}{[(P-k-q)^2 - M_K^2 + i\epsilon]},$$

where the driving term is

$$\xi_1(k) = -iW \int \frac{d^4q}{(2\pi)^4} \frac{1}{(q^2 - M_\pi^2 + i\epsilon)}$$
$$\times \frac{1}{[(P-k-q)^2 - M_K^2 + i\epsilon]}, \qquad (25)$$

and depends just on a one-loop integral. This term, multiplied by $T(m_{12}^2)$, gives rise to the first diagram in Fig. 7, whereas the second term in Eq. (25), multiplied by $T(m_{12}^2)$, represents the sum of all the remaining three-body connected processes shown in that figure. The lowest order connected contribution is the second diagram in Fig. 9.

The contribution to the three-body rescattering process given by Eq. (25) is built by mixing interactions from the two possible $K\pi$ pairs. The resulting reduced amplitude is a function of just the momentum of the final spectator-pion. The model separates the decay amplitude into two parts: one corresponding to a smooth function of the momenta of the pions in W and another given by $\xi(k)$ times the pair amplitude, which is a fully three-body interacting term modulated by the $K\pi$ amplitude.

So far, we did not consider isospin degrees of freedom. The kernel of the integral Eq. (25) involves the change between the pions corresponding to the final isospin channel of the pair $K\pi$ and gives rise to isospin factors discussed in Appendix B. The recoupling coefficient, given by Eq. (B3), appears weighting the kernel. Taking into account also the isospin weight for the driving term, we find

$$\xi(k) = \frac{5}{3}\xi_1(k) - \frac{2}{3}i \int \frac{d^4q}{(2\pi)^4} \frac{T[(P-q)^2]}{(q^2 - M_\pi^2 + i\epsilon)}$$
$$\times \frac{\xi(q)}{[(P-k-q)^2 - M_K^2 + i\epsilon]} \qquad (26)$$

As the main purpose of this work is to investigate the effect of the three-body unitarity on the decay amplitude, we analyze in the following section the perturbative contributions to the FSI at one- and two-loop approximations. We choose to exemplify the series expansion of Eq. (26) for the weak vertices a and c of Fig. 8 and present the case

of vertex b when discussing the perturbative calculation. In the case of vertex a, we find

$$A_a(m_{12}^2, m_{23}^2) = \sqrt{\frac{2}{3}}W_a \left\{ 1 + T(m_{12}^2)\frac{5}{3}\left[\xi_1(m_{12}^2) + \frac{2}{3}\xi_2(m_{12}^2) \right.\right.$$
$$\left.\left. + \left(\frac{2}{3}\right)^2 \xi_3(m_{12}^2)\cdots \right] \right\} + (1 \leftrightarrow 3), \qquad (27)$$

where the argument of the function ξ is written in terms of the invariant mass squared of the $K\pi$ subsystem, i.e. $m_{12}^2 = (P - p_3)^2$, instead of the individual momenta. The factor $\sqrt{\frac{2}{3}}$ comes from the isospin projection of the $K\pi$ pair in the weak vertices to $I = 1/2$. The perturbative n-loop amplitude is constructed recursively as

$$\xi_n[(P-k)^2] = -i \int \frac{d^4q}{(2\pi)^4} \frac{T[(P-q)^2]}{(q^2 - M_\pi^2 + i\epsilon)}$$
$$\times \frac{\xi_{n-1}[(P-q)^2]}{[(P-k-q)^2 - M_K^2 + i\epsilon]}. \qquad (28)$$

For later convenience, we introduce the function $\lambda_n(m_{12}^2)$, defined as

$$\lambda_n(m_{12}^2) = T(m_{12}^2)\xi_n(m_{12}^2), \qquad (29)$$

which is useful within our approximation of disregarding the momentum structure of the weak vertex, and Eq. (27) becomes

$$A_a(m_{12}^2, m_{23}^2) = \sqrt{\frac{2}{3}}W_a \left\{ 1 + \frac{5}{3}\left[\lambda_1(m_{12}^2) + \frac{2}{3}\lambda_2(m_{12}^2) \right.\right.$$
$$\left.\left. + \left(\frac{2}{3}\right)^2 \lambda_3(m_{12}^2)\cdots \right] \right\} + (1 \leftrightarrow 3). \qquad (30)$$

The three-body rescattering series starting from the weak vertex b has to be treated properly in order to avoid double counting in the scattering series in the two-meson channel, as the scalar resonance is dressed by the $K\pi$ interaction (c.f. Fig. 10). In the case of vertex c, the scattering series simplifies, as the π_0 produced directly from the W decay is not present in the final state, and it is written as
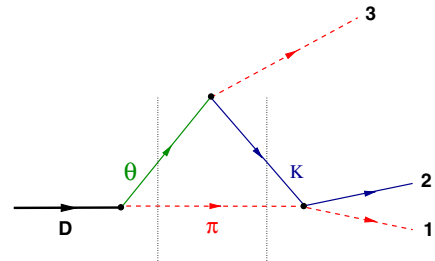

FIG. 10 (color online). Diagrams involving the weak vertex W_b; the wavy line is a W^+, always plugged to a π^+, and the dotted line is a scalar resonance, which has a width given by the substructure R described at the bottom line.

$$A_c(m_{12}^2, m_{23}^2) = -\frac{\sqrt{2}}{3} W_c \Big\{ \lambda_1(m_{12}^2) + \frac{2}{3}\lambda_2(m_{12}^2)$$
$$+ \Big(\frac{2}{3}\Big)^2 \lambda_3(m_{12}^2) \cdots \Big\} + (1 \leftrightarrow 3). \quad (31)$$

IV. PERTURBATIVE PROCESSES

In this section, the first two terms of the function $a(m_{12}^2)$ given by Eq. (22) are evaluated covariantly, and different contributions are classified according to the type of initial weak vertex. Diagrams involve two kinds of loops, containing either two- or three-meson propagators. The former require regularization and are treated as in the construction of the $K\pi$ amplitude presented in Sec. II. The latter are *triangle integrals*, written as

$$I_{\pi K \theta}(m_{12}^2) = \int \frac{d^4 k}{(2\pi)^4} \frac{1}{[(p_{12} - k)^2 - M_\pi^2 + i\epsilon]}$$
$$\times \frac{1}{[[k^2 - M_K^2 + i\epsilon](p_3 + k)^2 - \theta]}, \quad (32)$$

where $\theta = \theta_R - i\theta_I$ is the position of the pole in the complex s plane, with θ_R and θ_I constant positive quantities. This integral is similar to those occurring in usual calculations of form factors, but not identical, since the invariant masses along the dotted lines in Fig. 11 can be smaller than either m_D^2 or m_{12}^2. It is, thus, mathematically more akin to integrals needed to describe form factors of unstable particles, such as the Δ, ρ, or K^*. We write

$$I_{\pi K \theta} = i\Pi_{\pi K \theta}/(4\pi)^2, \quad (33)$$

and the evaluation of the functions Π is discussed in Appendix D.

A. Contributions proportional to W_a

Processes involving the weak vertex W_a, defined in Fig. 8, are indicated in Fig. 12. The W^+ is shown explicitly just for the sake of clarifying the various topologies and is taken as a point in calculations.

We start with the perturbative expansion given in Eq. (30), and we evaluate the one- and two-loop terms as
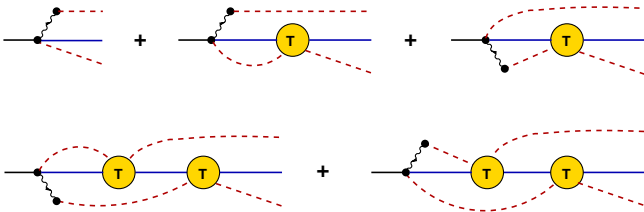

FIG. 11 (color online). Triangle diagram representing the reaction $D(P) \to [\pi K](p_{12})\pi(p_3)$, with intermediate states $\pi(p_{12} - k)$, $\theta(p_3 + k)$, $K(k)$, associated with the integral given in Eq. (32); invariant masses along the dotted lines can be smaller than those of external lines.
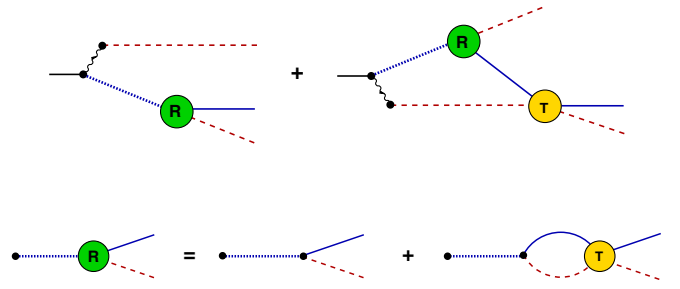

FIG. 12 (color online). Diagrams involving the weak vertex W_a; the wavy line is a W^+, always plugged to a π^+; the π produced, together with the $\bar{K}$, in the opposite side can be either positive or neutral.

follows. Using Eqs. (25) and (9), one gets $\xi_1(m_{12}^2) = -W_a \Omega(m_{12}^2)$ and $\lambda_1(m_{12}^2) = -T(m_{12}^2)\Omega(m_{12}^2)$. As Ω is divergent, a subtraction is needed, and we assume the subtraction constant to be the same as in the $K\pi$ scattering amplitude. Using Eq. (14), one has

$$\lambda_1(m_{12}^2) = -T(m_{12}^2)[C + \bar{\Omega}(m_{12}^2)] = -1 + \lambda_1'(m_{12}^2), \quad (34)$$

$$\lambda_1'(m_{12}^2) = 1/D(m_{12}^2). \quad (35)$$

Our assumption allows further simplifications in the treatment of the rescattering series, but it is still a freedom within our framework that we will not explore further, in order to minimize the number of free parameters in our first investigation of three-body rescattering effects.

The two-loop contribution comes from the recursive formula (28) and (29) and reads

$$\lambda_2(m_{12}^2) = iT(m_{12}^2) \int \frac{d^4 k}{(2\pi)^4} \frac{1}{[(p_{12} - k)^2 - M_\pi^2 + i\epsilon]}$$
$$\times \frac{1}{[k^2 - M_K^2 + i\epsilon]} T[(p_3 + k)^2]\Omega[(p_3 + k)^2], \quad (36)$$

and, again, the divergent function Ω shows up. Subtracting, we have

$$\lambda_2(m_{12}^2) = iT(m_{12}^2) \int \frac{d^4 k}{(2\pi)^4} \frac{1}{[(p_{12} - k)^2 - M_\pi^2 + i\epsilon]}$$
$$\times \frac{T[(p_3 + k)^2]}{[k^2 - M_K^2 + i\epsilon]} \{C + \bar{\Omega}[(p_3 + k)^2]\}. \quad (37)$$

Using Eq. (14) and subtracting once more, we get

$$\lambda_2(m_{12}^2) = T(m_{12}^2)[C + \bar{\Omega}(m_{12}^2)] + \lambda_2'(m_{12}^2)$$
$$= -\lambda_1(m_{12}^2) + \lambda_2'(m_{12}^2), \quad (38)$$

$$\lambda_2'(m_{12}^2) = -iT(m_{12}^2) \int \frac{d^4k}{(2\pi)^4} \frac{1}{[(p_{12}-k)^2 - M_\pi^2 + i\epsilon]}$$

$$\times \frac{1}{[k^2 - M_K^2 + i\epsilon]} \frac{1}{[D(p_3+k)^2]}. \quad (39)$$

Repeating this procedure for higher order loop contributions, we find the structure

$$\lambda_N(m_{12}^2) = -\lambda_{N-1}(m_{12}^2) + \lambda_N'(m_{12}^2), \quad (40)$$

which can be checked explicitly for λ_3 and λ_4, using the expressions shown in Appendix C. Denoting by S the sum of terms within the square bracket in Eq. (30), we have

$$S = \sum_{N=1}^\infty \left(\frac{2}{3}\right)^{N-1} \lambda_N = -\frac{2}{3}S - 1 + \sum_{N=1}^\infty \left(\frac{2}{3}\right)^{N-1} \lambda_N'. \quad (41)$$

This allows Eq. (30) to be expressed as

$$A_a(m_{12}^2, m_{23}^2) = \sqrt{\frac{2}{3}} W_a \left[\lambda_1'(m_{12}^2) + \frac{2}{3}\lambda_2'(m_{12}^2) \right. $$
$$\left. + \left(\frac{2}{3}\right)^2 \lambda_3'(m_{12}^2) + \cdots \right] + (1 \leftrightarrow 3). \quad (42)$$

This result is interesting and indicates the importance of treating both the $K\pi$ amplitude and the FSIs in a single coherent dynamical framework. The diagrams of Fig. 12 contribute to the first two terms of this series.

The integral (39) can be performed by a number of different techniques, provided one recalls that $1/D(s)$ contains two poles, associated with the κ and the $K^*(1430)$. One possibility would be to perform a Cauchy integration over k_0, supplemented by a numerical 3-dimensional integration. An alternative, adopted here, is to rely on usual Feynman techniques. With this purpose in mind, we employ the expression for the $K\pi$ amplitude written in terms of its poles, given in Eq. (19) and, using Eq. (32), obtain

$$\lambda_2'(m_{12}^2) = T(m_{12}^2)\{-\beta[C + \bar{\Omega}(m_{12}^2)] $$
$$+ \gamma_\kappa \Pi_{\pi K\theta_\kappa}/(16\pi^2) + \gamma_1 \Pi_{\pi K\theta_1}/(16\pi^2)\}. \quad (43)$$

The problem then reduces to the evaluation of triangle integrals.

B. Contributions proportional to W_b

We follow here the treatment of the production amplitude for a scalar resonance given in Ref. [43]. The basic idea is that processes, shown at the bottom line of Fig. 10, must always be considered together, since the tree contribution in isolation contains a pole in the physical region. The corresponding amplitude R^i, involving a resonance with mass m_i, reads
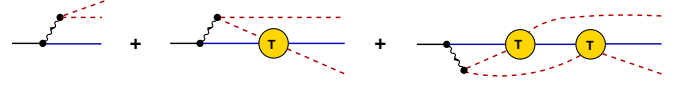

FIG. 13 (color online). Diagrams involving W_c; one of the pions in the weak vertex is neutral.

$$R^i(m_{12}^2) = -i\frac{1}{F^2}[c_d^i m_{12}^2 - (c_d^i - c_m^i)(M_\pi^2 - M_K^2)]$$
$$\times \frac{1}{m_{12}^2 - m_i^2}[1 - T(m_{12}^2)\Omega(m_{12}^2)]. \quad (44)$$

Regularizing the function Ω and using Eq. (14), one finds

$$R^i(m_{12}^2) = -i\frac{1}{F^2}[c_d^i m_{12}^2 - (c_d^i - c_m^i)(M_\pi^2 - M_K^2)]$$
$$\times \frac{1}{[m_{12}^2 - m_i^2]D(m_{12}^2)}. \quad (45)$$

This function is finite because, by construction, $D(m_i^2) = 0$.

The evaluation of the contributions to A_b is straightforward and yields

$$A_b = a_{b1} + a_{b2} + \cdots, \quad (46)$$

$$a_{b1}(m_{12}^2) = iW_b R^1(m_{12}^2), \quad (47)$$

$$a_{b2}(m_{12}^2) = W_b \frac{2}{3} T(m_{12}^2) \int \frac{d^4k}{(2\pi)^4} \frac{R^1(p_3+k)}{[(p_{12}-k)^2 - M_\pi^2 + i\epsilon]}$$
$$\times \frac{1}{[k^2 - M_K^2 + i\epsilon]}, \quad (48)$$

where the recursive formula (28) is used starting with $\xi_1(m_{12}^2) \equiv a_{b1}(m_{12}^2)$. The function a_{b2} can be reduced to a sum of triangle integrals and is evaluated using Eq. (32).

C. Contributions proportional to W_c

Processes given in Fig. 13 give rise to Eq. (31), which contains the same series as in Eq. (30). Using result (41), one finds

$$A_c(m_{12}^2, m_{23}^2) = -\frac{\sqrt{2}}{5} W_c \left[-1 + \lambda_1'(m_{12}^2) + \frac{2}{3}\lambda_2'(m_{12}^2) \right. $$
$$\left. + \left(\frac{2}{3}\right)^2 \lambda_3'(m_{12}^2) \cdots \right] + (1 \leftrightarrow 3). \quad (49)$$

V. RESULTS, CONCLUSIONS AND SUMMARY

In this work, we studied the role of final state interactions in $D^+ \rightarrow K^-\pi^+\pi^+$, treating two- and three-body interactions in a consistent way. Our underlying $K\pi$ amplitude is derived from chiral perturbation theory, supplemented by unitarization and tuned to elastic LASS data [1]. Two poles, associated with the κ and the $K^*(1430)$, were then determined and employed in a representation of the

amplitude. A number of simplifying assumptions were made in the $K\pi$ amplitude, for the sake of minimizing technical problems. Among them, we mention the absence of both isospin 3/2 and P waves, as well as couplings to vector mesons and to inelastic channels. The means for correcting these shortcomings are available in the literature and will be considered in future extensions of this work. Our treatment of three-body unitarity departs from a Faddeev-like integral equation, which is subsequently expanded perturbatively. Terms in the corresponding series contain a recursive component, which allows a resummation of the whole series, when the divergence is subtracted using the same criteria as in the $K\pi$ scattering amplitude.

Model independent analyses [8–10] of the S-wave $K^-\pi^+$ channel in the decay $D^+ \to K^-\pi^+\pi^+$ are rather welcome in theoretical studies because they are expressed in terms of amplitudes which are linear in the Fermi constant. This means that it is meaningful to study independently the strong evolution of each dynamical contribution to the primary weak vertex. In this work, we have considered just three simple topologies of the color-allowed type to the primary vertex, which yield classes of decay amplitudes denoted by $A_a, A_b,$ and A_c (42) and (47)–(49). The first two begin at tree level and give rise to quasi two-body FSIs, as in Ref. [25]. The amplitude A_c, on the other hand, arises only when proper three-body FSIs are present.

Predictions for their modulus are given in Figs. 14. It is important to note that the order N of partial contributions indicates the number of times the denominator $1/D$ of Eq. (14) intervenes in a given function. Results for A_a and A_c, in particular, are based on an infinite resummation of terms, Eq. (41), and hence N is *not* simply related with perturbative counting. Understood in this sense, second order terms tend to be smaller that leading ones. However, in the case of A_a and A_c, FSI corrections show up clearly around the bare resonance mass, where the function $1/D$ vanishes along the real axis. In the case of A_b, one notices a cancellation close to threshold. As far as comparison with FOCUS data [9] is concerned, we note that A_c has a dip at the correct position, whereas compatibility with the direct production of a resonance at the weak vertex is very difficult.

Predictions for the phase are displayed in Fig. 15. Contribution from λ'_1 in Eq. (42) and (49) and from a_{b1} in Eq. (47) falls exactly over the elastic $K\pi$ phase. The oscillation in A_b at low energies can be ascribed to the lack of precision in a_{b2}. We have checked that it is due to an incomplete cancellation between a precise tree term and the less-precise triangle contribution in processes shown in Fig. 10. Finally, we see that a curve for A_c, shifted by -148^0, describes well FOCUS data [9] up to the region of the peak.

As the study of both the modulus and the phase seems to favor the weak vertex W_c of Fig. 8, it is worth exploring its structure. In Fig. 16, we show the phases of the factors $-1 + \lambda'_1(m_{12}^2)$ and $-1 + \lambda'_1(m_{12}^2) + \frac{2}{3}\lambda'_2(m_{12}^2)$ in Eq. (49). The gap between them is about 10^0, and the first term already corresponds to a good approximation to low-energy FOCUS data. However, as pointed out above, the factor -1 in these terms comes from an infinite resummation, and, hence, the smallness of this gap *does not* indicate that it is enough to consider just the first perturbative contribution. Using Eqs. (49), (35), and (12), one has
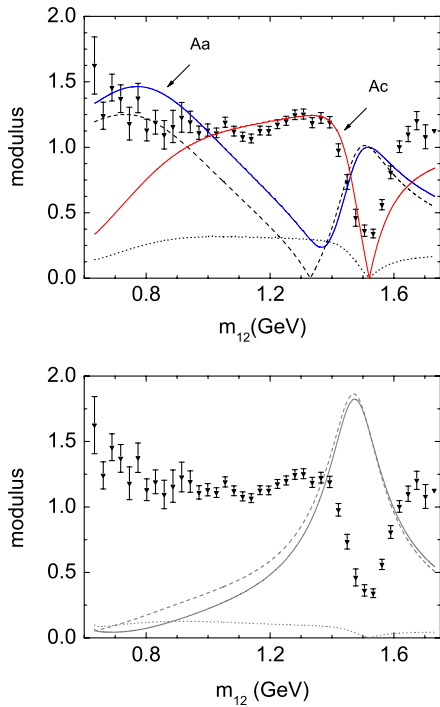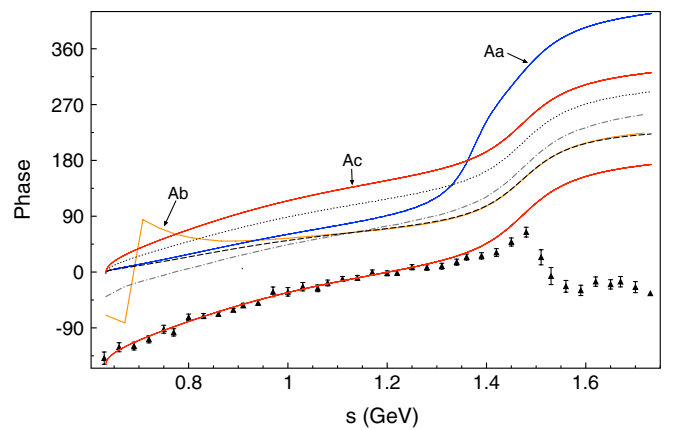

FIG. 14 (color online).   Top: behavior of $|A_a|$ and $|A_c|$; bottom: behavior of $|A_b|$; first and second order partial contributions are indicated by dashed and dotted lines.

FIG. 15 (color online).   Phases from A_a, A_b, and A_c (continuous line); partial contributions from λ'_1 in Eqs. (42) and (49) and from a_{b1} in Eq. (47) coincide with the elastic $K\pi$ phase (dashed lines); contributions from λ'_2 and a_{b2} are given, respectively, by dotted and dashed-dotted lines; the curve coinciding partially with FOCUS data [9] (triangle) is A_c, shifted by -148^0.
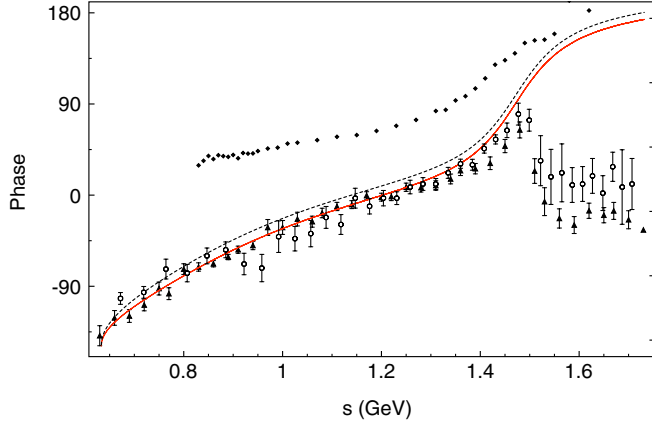
FIG. 16 (color online). Phases of the factors $-1 + \lambda'_1(m^2_{12})$ (dashed) and $-1 + \lambda'_1(m^2_{12}) + \frac{2}{3}\lambda'_2(m^2_{12})$ (continuous) in Eq. (49), shifted by -148^0, compared with FOCUS [9] (triangle) and E791 [8] (circle) data, together with elastic $K\pi$ results from LASS [1] (diamond).
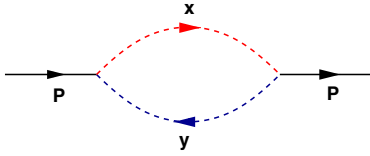

FIG. 17 (color online). Bubble loop diagram.

$$A_c(m^2_{12}, m^2_{23}) \simeq -\frac{\sqrt{2}}{5} W_c \left[-1 + \frac{1}{1 + (C + \bar{\Omega})\mathcal{K}} \right] + (1 \leftrightarrow 3),$$
(50)

where $\mathcal{K}$ is the $K\pi$ kernel of Eq. (5). Hence, the dip in experimental results for the magnitude of A indicates the energy at which $\mathcal{K} = 0$. In our model, this corresponds to the point where both the real and imaginary parts of the scattering amplitude cross the real axis in Fig. 5.

In this framework, Eq. (50), rewritten as

$$A_c(m^2_{12}, m^2_{23}) \simeq \frac{\sqrt{2}}{5} W_c \left[\frac{(C + \bar{\Omega})\mathcal{K}}{1 + (C + \bar{\Omega})\mathcal{K}} \right] + (1 \leftrightarrow 3), \quad (51)$$

could provide a much more convenient structure to be used in experimental analyses, since $\bar{\Omega}$ is a well-known elementary function.

As stressed before, this work concentrates at tracking leading effects, and a number of important issues were left untouched. Among them, we mention the absence of P waves, isospin 3/2 terms, and inelastic contributions to the basic $K\pi$ amplitude, as well as a more complete description of the primary weak vertex. These matters will be dealt with in other papers.

In summary, our main conclusions read:

(1) proper three-body effects are important;

(2) corrections to the resummed series are important at threshold and fade away rapidly at higher energies;

(3) a model based on a vector-weak vertex can describe qualitative features of the modulus from FOCUS and E791 data [8,9] for the decay amplitude and agrees well with its phase in the elastic region.

ACKNOWLEDGMENTS

APPENDIX A: TWO-MESON PROPAGATOR

The basic process is shown in Fig. 17, and the corresponding integral is

$$I_{\pi K}(s) = \int \frac{d^4\ell}{(2\pi)^4} \frac{1}{[(\ell + p/2)^2 - M^2_\pi][(\ell - p/2)^2 - M^2_K]}$$
$$= \frac{i}{(4\pi)^2} \Pi^{00}_{xy}(s), \tag{A1}$$

since $P^2 = s$. In the Bethe-Salpeter equation, it is convenient to use

$$\Omega(s) \equiv i I_{\pi K}(s) \equiv -[L(s) + \Lambda_\infty]/16\pi^2, \tag{A2}$$

where $L(s)$ is a finite function and Λ_∞ incorporates the ultraviolet divergence. The regular part of Ω is defined as

$$\bar{\Omega}(s) = \Omega(s) - \Omega(0) = -[L(s) - L(0)]/16\pi^2$$
$$= -\bar{L}(s)/16\pi^2, \tag{A3}$$

where,

(i) $s < (M_\pi - M_K)^2$

$$\bar{L} = \check{L} + \frac{\sqrt{\lambda}}{s} \ln\left[\frac{M^2_\pi + M^2_K - s + \sqrt{\lambda}z}{2M_\pi M_K}\right], \quad (A4)$$

(ii) $(M_\pi - M_K)^2 < s < (M^2_\pi + M^2_K)$

$$\bar{L} = \check{L} - \frac{\sqrt{-\lambda}}{s} \tan^{-1}\left[\frac{\sqrt{-\lambda}}{M^2_\pi + M^2_K - s}\right], \quad (A5)$$

(iii) $(M^2_\pi + M^2_K) < s < (M_\pi + M_K)^2$

$$\bar{L} = \check{L} - \frac{\sqrt{-\lambda}}{s}\left\{\tan^{-1}\left[\frac{\sqrt{-\lambda}}{M^2_\pi + M^2_K - s}\right] + \pi\right\},$$
(A6)

(iv) $s > (M_\pi + M_K)^2$

$$\bar{L} = \check{L} - \frac{\sqrt{\lambda}}{s} \ln\left[\frac{s - M_\pi^2 - M_K^2 + \sqrt{\lambda}}{2M_\pi M_K}\right] + i\pi\frac{\sqrt{\lambda}}{s},$$

(A7)

with

$$\check{L} = 1 + \frac{M_\pi^2 + M_K^2}{M_\pi^2 - M_K^2}\ln\left[\frac{M_\pi}{M_K}\right] - \frac{M_\pi^2 - M_K^2}{s}\ln\left[\frac{M_\pi}{M_K}\right],$$

(A8)

$$\lambda = s^2 - 2s(M_\pi^2 + M_K^2) + (M_\pi^2 - M_K^2)^2.$$ (A9)

APPENDIX B: ISOSPIN IN FSIS

In order to derive the isospin weighting factors presented in the integral equation (26), one has to realize that the adopted model for the $K\pi$ transition matrix has a separable form, which allows the factorization of the decay amplitude as given by Eq. (24). In addition, we consider only the dominant isospin $1/2$ channel of the $K\pi$ system. The isospin $1/2$ dependence in the transition matrix is made explicit by writing it as

$$T_{1/2} \equiv \sum_{i_z}|I_{K\pi} = 1/2, i_z\rangle T\langle I_{K\pi} = 1/2, i_z|,$$ (B1)

where the matrix element of T is given by Eq. (19).

The $K\pi\pi$ scattering amplitude with $I_z = 3/2$ is built only with total isospin states $I_T = 3/2$, because the $K\pi$ subsystem interacts only in the isospin doublet channel. The states with isospin $5/2$ do not contribute to the final state interaction in our model. The above simplification implies that the spectator function ξ, which also carries the bachelor pion momentum distribution, is given by

$$|\xi_{3/2}(k_\pi)\rangle = |I_T, I_z, I_\pi, I_{K\pi'}\rangle\xi(k_\pi),$$ (B2)

where $I_T = 3/2$, $I_z = 3/2$, $I_\pi = I_{\pi'} = 1$ and $I_{K\pi} = I_{K\pi'} = 1/2$.

Following the diagrammatic representation of the integral equation (25) shown in Fig. 9, one realizes that the kaon is exchanged between the two possible interacting $K\pi$ pairs. Guided by the diagram, one verifies that the bachelor pion in the intermediate state interacts with the kaon and forms a new pair. This is a known property of the Faddeev decomposition, which equates only different Faddeev components of the $3 \rightarrow 3$ transition matrix.

The kernel of the integral equation exchanges the role of the bachelor pions from the intermediate to the final state (see Fig. 9). In addition, by considering the $I = 1/2$ transition amplitude (B1) and the isospin structure of the spectator function (B2), one finds that the weighting isospin factor multiplying the kernel of Eq. (26) is given by the recoupling coefficient

$$R_{3/2} \equiv \langle I_T, I_z, I_\pi, I_{K\pi'}|I_T, I_z, I_{\pi'}, I_{K\pi}\rangle,$$ (B3)

which is written in terms of Wigner 6-j symbol,

$$R_{3/2} = (-1)^S f(I_{K\pi})f(I_{K\pi'})\begin{Bmatrix} I_\pi & I_K & I_{K\pi} \\ I_\pi & I_T & I_{K\pi'} \end{Bmatrix},$$ (B4)

with $S = 2I_\pi + I_K + I_T$ and $f(I) = \sqrt{2I + 1}$. The result is the weight factor $R_{3/2} = 2/3$ in Eq. (26).

In the particular case of Eq. (26), the driving term for $I_T = 3/2$ is derived from a weak vertex symmetric under the exchange of the pions, such that

$$|W_{3/2}\rangle = W(|I_T, I_z, I_\pi, I_{K\pi'}\rangle + |I_T, I_z, I_{\pi'}, I_{K\pi}\rangle).$$ (B5)

Both terms contribute to the driving term isospin weighting factor after projection onto the appropriate isospin state, which corresponds to the spectator function (B2). One gets that

$$\langle I_T, I_z, I_\pi, I_{K\pi'}|W_{3/2}\rangle = W\langle I_T, I_z, I_\pi, I_{K\pi'}|I_T, I_z, I_\pi, I_{K\pi'}\rangle$$
$$+ W\langle I_T, I_z, I_\pi, I_{K\pi'}|I_T, I_z, I_{\pi'}, I_{K\pi}\rangle$$
$$= \frac{5}{3}W,$$ (B6)

which was computed by using the isospin recoupling coefficient (B4).

APPENDIX C. PERTURBATIVE CONTRIBUTIONS

Perturbative contributions to the FSI amplitude $a(m_{12}^2) = \sum_{N=1}^{\infty} a_N(m_{12}^2)$, Eq. (22), have the structure

$$a_N(m_{12}^2) = -a_{N-1}(m_{12}^2) + a_1(m_{12}^2)\lambda_N(m_{12}^2),$$ (C1)

and, in the sequence, we list the $\lambda_N'(m_{12}^2)$ for $N = 3, 4$.

$$\lambda_3'(m_{12}^2) = -T(m_{12}^2)\int\frac{d^4k}{(4\pi)^4}\frac{1}{(p_{12} - k)^2 - M_\pi^2 + i\epsilon}\frac{1}{k^2 - M_K^2 + i\epsilon}T(k + p_3)$$
$$\times \int\frac{d^4k'}{(4\pi)^4}\frac{1}{[(k + p_3) - k']^2 - M_\pi^2 + i\epsilon}\frac{1}{k'^2 - M_K^2 + i\epsilon}\frac{1}{D[(k' + p_{12} - k)^2]},$$ (C2)

$$\lambda'_4(m^2_{12}) = iT(m^2_{12}) \int \frac{d^4k}{(4\pi)^4} \frac{1}{(p_{12}-k)^2 - M^2_\pi + i\epsilon} \frac{1}{k^2 - M^2_K + i\epsilon} T(k+p_3) \int \frac{d^4k'}{(4\pi)^4} \frac{1}{[(k+p_3)-k']^2 - M^2_\pi + i\epsilon}$$

$$\times \frac{1}{k'^2 - M^2_K + i\epsilon} T[(p_{12}-k)+k'] \int \frac{d^4k''}{(4\pi)^4} \frac{1}{\{[k'+(p_{12}-k)]-k''\}^2 - M^2_\pi + i\epsilon} \frac{1}{k''^2 - M^2_K + i\epsilon}$$

$$\times \frac{1}{D[(p_3 + k - k' + k'')^2]}. \tag{C3}$$

APPENDIX D: TRIANGLE INTEGRAL

The triangle integral defined by Eq. (32) and represented in Fig. 11 is written as

$$I_{\pi K\theta} = \frac{i}{(4\pi)^2} \Pi_{\pi K\theta} = -\frac{i}{(4\pi)^2} \int_0^1 da\, a \int_0^1 db\, \frac{1}{D_{\pi K\theta}}, \tag{D1}$$

$$D_{\pi K\theta} = (1-a)M^2_\pi + a(1-b)M^2_K + ab\theta_R - i[\epsilon + ab(\theta_I - \epsilon)] - a(1-a)(1-b)m^2_{12} - a(1-a)bM^2_D - a^2b(1-b)M^2_\pi. \tag{D2}$$

The double integral (D1) can be evaluated numerically but, in the case $\theta_I = \epsilon$, problems of accuracy may arise. In order to understand the structure of its complex part, it is desirable to pursue the analytic path as long as possible. We, therefore, resort to the $SU(2)$ chiral limit and neglect M^2_π, eliminating terms proportional to b^2 in $D_{SK\pi}$ and simplifying the algebra. Integration in b yields

$$J = \int_0^1 db\, \frac{a}{D_{\pi K\theta}}$$

$$= \frac{G + i(\theta_I - \epsilon)}{G^2 + (\theta_I - \epsilon)^2} \left\{ \frac{1}{2} \ln\frac{[F+G]^2 + [(\theta_I - \epsilon) + \epsilon/a]^2}{F^2 + (\epsilon/a)^2} \right.$$

$$\left. - i\frac{F(\theta_I - \epsilon) - G(\epsilon/a)}{|F(\theta_I - \epsilon) - G(\epsilon/a)|} \left[\tan^{-1}\frac{x-y}{1+xy} + \sigma\pi \right] \right\},$$

$$F = M^2_K - (1-a)m^2_{12}, \qquad G = (\theta_R - M^2_K) - (1-a)(M^2_D - m^2_{12}),$$

$$x = \frac{(F+G)G + (\theta_I - \epsilon)(\theta_I - \epsilon + \epsilon/a)}{|F(\theta_I - \epsilon) - G(\epsilon/a)|}, \qquad y = \frac{FG + (\theta_I - \epsilon)(\epsilon/a)}{|F(\theta_I - \epsilon) - G(\epsilon/a)|}, \tag{D3}$$

with $[xy > -1] \rightarrow \sigma = 0$, $[xy < -1 \text{ and } x > 0] \rightarrow \sigma = +1$, $[xy < -1 \text{ and } x < 0] \rightarrow \sigma = -1$. This result was used to tune numerical calculations, and one found that convergence for small values of ϵ requires a large number of points in a Gaussian integration.

[1] D. Aston *et al.*, Nucl. Phys. **B296**, 493 (1988); P. Estabrooks *et al.*, *ibid.* **B133**, 490 (1978).

[2] E. M. Aitala *et al.* (E791 collaboration), Phys. Rev. Lett. **86**, 770 (2001); **86**, 765 (2001).

[3] E. M. Aitala *et al.* (E791 collaboration), Phys. Rev. Lett. **89**, 121801 (2002).

[4] P. del Amo Sanchez *et al.* (*BABAR* Collaboration), Phys. Rev. D **83**, 072001 (2011).

[5] J. M. Link *et al.* (FOCUS Collaboration), Phys. Lett. B **621**, 72 (2005).

[6] S. Paramesvaran *et al.* (*BABAR* Collaboration), in Division of Particles and Fields 2009, Detroit, Michigan, 2009, eConf C090726, (2009) arXiv:hep-ex0910.2884.

[7] D. Epifanov *et al.* (Belle Collaboration), Phys. Lett. B **654**, 65 (2007).

[8] E. M. Aitala *et al.* (E791 Collaboration), Phys. Rev. D **73**, 032004 (2006); **74**, 059901 (2006).

[9] J. M. Link *et al.* (FOCUS Collaboration), Phys. Lett. B **681**, 14 (2009).

[10] G. Bonvicini *et al.* (CLEO-c Collaboration), Phys. Rev. D **78**, 052001 (2008).

[11] G. Burdman and J. F. Donoghue, Phys. Lett. B **280**, 287 (1992); M. B. Wise, Phys. Rev. D **45**, R2188 (1992); R. Casalbuoni, A. Deandrea, N. Di Bartolomeo, R. Gatto, F. Feruglio, and G. Nardulli, Phys. Rep. **281**, 145 (1997); M. Diakonou and F. Diakonos, Phys. Lett. B **216**, 436 (1989).

[12] Ya. Azimov, J. Phys. G **37**, 023001 (2010).

[13] I. Caprini, Phys. Lett. B **638**, 468 (2006).

[14] Bochao Liu, Markus Buescher, Feng-Kun Guo, Christoph Hanhart, and Ulf-G. Meissner, Eur. Phys. J. C **63**, 93 (2009).

[15] Ulf-G. Meissner and Susan Gardner, Eur. Phys. J. A **18**, 543 (2003).

[16] K. S. F. F. Guimarães, W. de Paula, I. Bediaga, A. Delfino, T. Frederico, A. C. dos Reis, and L. Tomio, Nucl. Phys. B, Proc. Suppl. **199**, 341 (2010).

[17] Z-Y. Zhou, Q-C. Wang, and Q. Gao, Chinese Phys. C **35**, 708 (2011).

[18] A. Stadler and F. Gross, Few-Body Syst. **49**, 91 (2010).

[19] W. N. Polyzou, Ch. Elster, W. Glöckle, J. Golak, Y. Huang, H. Kamada, R. Skibiński, and H. Witala, Few-Body Syst. **49**, 129 (2010).

[20] E. P. Biernat, W. H. Klink, and W. Schweiger, Few-Body Syst. **49**, 149 (2010).

[21] T. Frederico and G. Salmè, Few-Body Syst. **49**, 163 (2010).

[22] J. Carbonell and V. A. Karmanov, Few-Body Syst. **49**, 205 (2010).

[23] V. Sauli, Few-Body Syst. **49**, 223 (2010).

[24] S. M. Dorkin, L. P. Kaptari, C. Ciofi degli Atti, and B. Kämpfer, Few-Body Syst. **49**, 233 (2010).

[25] D. R. Boito and R. Escribano, Phys. Rev. D **80**, 054007 (2009).

[26] I. Bediaga, C. Gobel, and R. Méndez-Galain, Phys. Rev. Lett. **78**, 22 (1997).

[27] J. Gasser and H. Leutwyler, Nucl. Phys. **B250**, 465 (1985); Ann. Phys. **158**, 142 (1984).

[28] G. Ecker, J. Gasser, A. Pich, and E. De Rafael, Nucl. Phys. **B321**, 311 (1989).

[29] K. Nakamura *et al.* (Particle Data Group), J. Phys. G **37**, 075021 (2010).

[30] M. Ablikim *et al.* (BES Collaboration), Phys. Lett. B **633**, 681 (2006).

[31] E. van Beveren, T. A. Rijken, K. Metzger, and C. Dullemond, Z. Phys. C **30**, 615 (1986); S. Ishida, M. Ishida, T Ishida, K. Takamatsu, and T. Tsuru, Prog. Theor. Phys. **98**, 621 (1997); D. Black, A. H. Fariborz,F. Sannino, and J. Schechter, Phys. Rev. D **58**, 054012 (1998); D. V. Bugg, Phys. Lett. B **572**, 1 (2003); , AIP Conf. Proc. **1030**, 379 (2008).Z. Y. Zhout and H. Q. Zheng, Nucl. Phys. **A775**, 212 (2006).

[32] J. A. Oller and E. Oset, Phys. Rev. D **60**, 074023 (1999); Nucl. Phys. **A620**, 438 (1997); **A652**, 407(E) (1999).

[33] M. Jamin, J. A. Oller, and A. Pich, Nucl. Phys. **B587**, 331 (2000); Phys. Rev. D **62**, 093013 (2000).

[34] P. Büttiker, S. Descotes-Genon, and B. Moussallam, Eur. Phys. J. C **33**, 409 (2004).

[35] J. R. Peláez, Mod. Phys. Lett. A **19**, 2879 (2004).

[36] T. V. Brito, F. S. Navarra, M. Nielsen, and M. E. Bracco, Phys. Lett. B **608**, 69 (2005);

[37] G. t Hooft, G. Isidori, L. Maiani, A. D. Polosa, and V. Riquer, Phys. Lett. B **662**, 424 (2008).

[38] W. de Paula, T. Frederico, H. Forkel, and M. Beyer, Phys. Rev. D **79**, 075019 (2009); W. de Paula and T. Frederico, Phys. Lett. B **693**, 287 (2010).

[39] G. Colangelo, J. Gasser, and H. Leutwyler, Nucl. Phys. **B603**, 125 (2001); H. Leutwyler, AIP Conf. Proc. **1030**, 46 (2008).

[40] J. Sa Borges, J. Barbosa Soares, and V. Oguri, Phys. Lett. B **412**, 389 (1997).

[41] L.-L. Chau, Phys. Rep. **95**, 1 (1983).

[42] Bauer, Stech, and Wirbel, Z. Phys. C **34**, 103 (1987).

[43] D. R. Boito and M. R. Robilotta, Phys. Rev. D **76**, 094011 (2007).